Organic Process Research & Development **2010,** *14,* 524–536

Nonisothermal Calorimetry for Fast Thermokinetic Reaction Analysis: Solvent-Free Esterification of *n*-Butanol by Acetic Anhydride

Gilles Richner, Yorck-Michael Neuhold,* and Konrad Hungerbühler

Institute for Chemical and Bioengineering, Department of Chemistry and Applied Biosciences, ETH Zurich, Hönggerberg HCI, 8093 Zurich, Switzerland

Abstract:

An enhanced small-scale reaction calorimeter has been built for nonisothermal applications. Its unique design, combining compensation heater and heat flow sensors together with a solid intermediate thermostat is particularly suited for data oriented process development (determination of chemical reaction parameters, i.e. rate constants, reaction enthalpies, and reaction monitoring with optional in situ devices) in a wide range of applications in chemical and life-science oriented industries.The performance of the calorimeter is successfully demonstrated for kinetic investigation under nonisothermal conditions. Three different methods for determining the time-resolved reaction heat have been tested. The first is based on the traditional heat balance, the second on the twin principle, while the third is a novel method based on a rigourous heat flow modelling using mathematical finite methods. As a case study, we investigated the esterification of *n*-butanol with acetic anhydride catalysed by tetramethylguanidine using a temperature ramp from 30 to 80 °C. Each method accounts differently for the dynamics and the heat accumulation in the system. However, all three methods show minor differences in the resulting kinetic parameters and reaction enthalpies. In this temperature range, kinetic and mechanistic analysis resolved two competitive parallel catalytic and noncatalytic steps.

Introduction

During early stages of process development chemical and pharmaceutical industry needs flexible and versatile tools to assess information about chemical reaction systems. For several decades, calorimetry has become a standard analytical technique in laboratories for monitoring the heat liberated or absorbed by chemical and biological reactions. Reaction calorimetry (RC) allows simulating industrial plants at a litre-scale, including dosing, mixing, and controlling of the reactor temperature and/or pressure,[1] and using simultaneously multiple in situ analytical devices. RC has been successfully employed during process development for investigation of thermal safety[2,3] but also to elucidate reaction mechanisms and associated activation energies, rate constants, and heats of reaction,[4,5] and to optimise chemical processes in a data oriented way.

Several publications are dedicated to reaction calorimeters, reviewing their different principles (*power compensation*, *heat flow*, and *heat balance*), and their operational modes (*adiabatic*, *isoperibolic*, *isothermal*, *temperature modulations*, and *Peltier*).[2,6–8] Isothermal mode is often preferred to reduce the amount of information to be interpreted (e.g., temperature dependency of the chemical system).[8] However, temperature modulations (mostly temperature ramps) are widely used for crystallisation[9] and polymerisation.[10] Moreover, for simple reactions, the activation energy, E_a, can be determined simultaneously to the reaction enthalpy, $\Delta_r H$, and the pre-exponential factor of the Arrhenius equation in one single nonisothermal experiment,[11] while the usual approach requires to perform the reaction at several different temperatures to draw an Arrhenius plot.[12] That way, a considerable gain of time and of test substance is expected. However, it is well-known that the determination of the reaction heat during a temperature ramp is a challenging task as the temperature ramp often shifts the baseline of the heat signals due to temperature dependencies of the overall heat transfer coefficient, the heat loss, and/or because heat may undesirably accumulate into the system[11,13] and may require several time-consuming calibrations.

To compensate for baseline shift due to the system itself, twin-system calorimeters, such as a Differential Scanning Calorimeter (DSC)[14] or a Differential Reaction Calorimeter (DRC),[15] have been designed for the differential measurement principle such that a sample vessel and a reference vessel run in parallel. Naturally, for a good consideration of the dynamics of the system, the physical properties of the reference should be close to those of the sample. In a single vessel, a similar approach consists of repeating the measurement with a nonreactive reference.[16]

* Author to whom correspondence may be sent. E-mail: bobby.neuhold@chem.ethz.ch.

(1) Ferguson, H. F.; Frurip, D. J.; Pastor, A. J.; Peerey, L. M.; Whiting, L. F. *Thermochim. Acta* **2000**, *363*, 1–21.
(2) Regenass, W. *J. Therm. Anal.* **1997**, *49*, 1661–1675.
(3) Stoessel, F. *J. Therm. Anal.* **1997**, *49*, 1677–1688.
(4) Regenass, W. *Thermochim. Acta* **1977**, *20*, 65–79.
(5) Fischer, U.; Hungerbühler, K. In *The Investigation of Organic Reactions and Their Mechanisms*; Maskill, H., Ed.; Blackwell: Oxford, UK, 2006; pp 198−226.
(6) Karlsen, L. G.; Villadsen, J. *Chem. Eng. Sci.* **1987**, *42*, 1153–1164.
(7) Landau, R. *Thermochim. Acta* **1996**, *289*, 101–126.
(8) Zogg, A.; Stoessel, F.; Fischer, U.; Hungerbühler, K. *Thermochim. Acta* **2004**, *419*, 1–17.
(9) Monnier, O.; Fevotte, G.; Hoff, C.; Klein, J. P. *Chem. Eng. Sci.* **1997**, *52*, 1125–1139.
(10) Grolier, J.-P. E.; Dan, F. *Thermochim. Acta* **2006**, *450*, 47–55.
(11) Hoffmann, W.; Kang, Y.; Mitchell, J. C.; Snowden, M. J. *Org. Process Res. Dev.* **2007**, *11*, 25–29.
(12) Pastré, J.; Zogg, A.; Fischer, U.; Hungerbühler, K. *Org. Process Res. Dev.* **2001**, *5*, 158–166.
(13) Weisenburger, G. A.; Barnhart, R. W.; Clark, J. D.; Dale, D. J.; Hawksworth, M.; Higginson, P. D.; Kang, Y.; Knoechel, D. J.; Moon, B. S.; Shaw, S. M.; Taber, G. P.; Ticknert, D. L. *Org. Process Res. Dev.* **2007**, *11*, 1112–1125.
(14) Lacey, A. A.; Price, D. M.; Reading, M. In *Modulated-Temperature Differential Scanning Calorimetry*; Reading, M., Hourston, D. J., Eds.; Springer: Netherlands, 2006; pp 1−81.
(15) André, R.; Bou-Diab, L.; Lerena, P.; Stoessel, F.; Giordano, M.; Mathonat, C. *Org. Process Res. Dev.* **2002**, *6*, 915–921.

10.1021/op900298x © 2010 American Chemical Society
Published on Web 05/03/2010

Scheme 1. **Esterification of *n*-butanol (BuOH) by acetic anhydride (AA), catalysed by 1,1,3,3-tetramethylguanidine (TMG)**

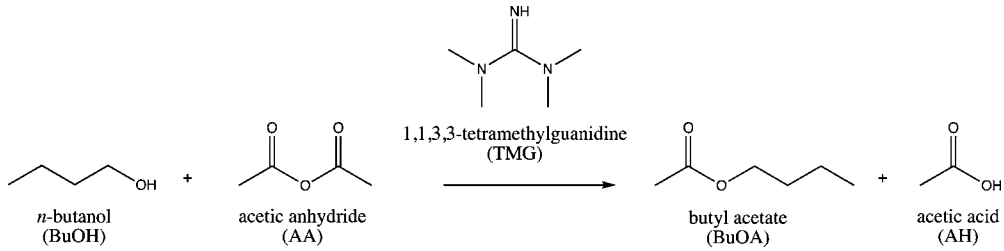

To study reaction mechanisms, in situ IR-spectroscopy is often preferred to calorimetry. Multivariate spectra provide more information on the chemical system, and optimisation of the kinetic parameters is more robust than the monovariate calorimetric data. However, under nonisothermal conditions, the validity of Lambert−Beer's law is often limited due to temperature dependent spectral shifts in the absorbance spectra.[17]

The goal of this study is to demonstrate that nonisothermal calorimetric investigations without time-consuming calibration steps may provide quick kinetic and mechanistic information without performing an extensive kinetic study. To do so, we first test the performance of our reaction calorimeter to control the reaction temperature under nonisothermal conditions, since until now, our prototype calorimeter has been used under strictly isothermal conditions only. As a case study, the kinetics of the solvent-free base-catalysed esterification of *n*-butanol by acetic anhydride is reinvestigated. We applied three different methods to perform the heat balance. The first two methods have been already commonly used and employ either a global heat balance or a measured reference. In the third method, we present a novel approach based on a heat flow model of our reactor and a simulated blank. Kinetic modelling with only few nonisothermal measurements indicate a mechanism of two competitive parallel reactions.

Experimental Section

Reaction. Ecological impact from chemical and pharmaceutical industry has been gradually decreasing during the past few years, encouraged by political decisions for CO_2 reduction factors. Solvent-free reaction environment is a promising solution to produce chemicals under green conditions as pre- and post- treatment of solvent (purification, separation and recycling) can be avoided. However, as no thermal buffer and high chemical concentrations are present, the reaction has to be particularly well-characterised. As an example, we investigated the solvent-free esterification of *n*-butanol (BuOH) by acetic anhydride (AA), catalysed by 1,1,3,3-tetramethylguanidine (TMG) to form butyl acetate (BuOA) and acetic acid (AH), Scheme 1. This reaction is of particular relevance in industry for solvent, pharmaceutical, perfume and explosive manufacturing.

Few studies showed that an autocatalytic behaviour of esterification between anhydrides and alcohols[18] may lead to several safety issues. For example, in case of thermal runaway, the boiling point of the reaction mixture may be reached increasing dangerously the pressure of the reactor.[19] To our knowledge, only few investigations studied the base-catalysed esterification, and the researchers reported mainly a pseudo-second-order reaction mechanism, with[20] or without[21,22] fast equilibrium of an activated catalyst complex. All these studies were performed below 50 °C under multiple isothermal conditions. In the present study, we investigated the reaction from 30 to 80 °C to cover also the temperature range reported in literature for the esterification of acetic anhydride by methanol.[18]

The experiments were carried out in a semibatch mode using the following procedure. The reactor was initially flushed with dry N_2 and then loaded with 22 mL of acetic anhydride (Acros Organics, 99+%) and 1.25 mL of 1,1,3,3-tetramethylguanidine (ABCR-Chemicals, 99%). After the steady-state has been reached (T_r = 30 °C), 21.4 mL of *n*-butanol (Acros Organics, 99%, extra pure) was fed at 3 mL/min with a syringe pump (kdS 200, kdScientic) and a gastight Hamilton syringe (series 1000, 25 mL). The temperature ramp was started after the end of the dosing to avoid perturbance by heat of mixing during the nonisothermal phase. The ramp was applied simultaneously to the temperatures of the reactor, T_r, the jacket, T_j and the cover, T_{cover} (see Figure 1). A heating rate of 1 °C/min was chosen in line with typical heating rates reported in literature[11,16] and also due to limitation in the temperature control of the cover, T_{cover}. An overview of the reaction conditions is given in Table 1.

Instrumentation. All experiments were performed in a high performance small-scale reaction calorimeter, which has been under ongoing development in our laboratories for the last 10 years. As illustrated in Figure 1, the system is composed of one stirred vessel (in Hastelloy) and a hexagonal metal jacket (in copper) designed as an intermediate thermostat. The jacket temperature is controlled by six Peltier elements (Melcor, HT 6-12-40-T2) placed on the lateral sides of the jacket. The heat pumped through the Peltiers is carried away by coolers connected to a cryostat (Haake P1-C50P). The temperature of the bulk is controlled by an electric compensation heater, whose power varies as the reaction liberates or consumes energy. Sample volumes of 20−50 mL bridge the gap between commercially available reaction calorimeters typically working in the one-litre scale, and microvolume thermo-analytical instruments. Thus, the device is particularly useful for research

(16) Bickerton, J.; Timms, A. W. In *Hazards XVI: Analysing the Past, Planning the Future*; Pantony, M. F., Ed.; Institution of Chemical Engineers (IChemE): Manchester, UK, 2001; pp 109−123.
(17) Zogg, A.; Fischer, U.; Hungerbühler, K. *Chem. Eng. Sci.* **2004**, *59*, 5795–5806.
(18) Widell, R.; Karlsson, H. T. *Thermochim. Acta* **2006**, *447*, 57–63.
(19) Gibson, N.; Roger, R.; Wright, T. *Inst. Chem. Eng. Symp. Ser.* **1987**, *102*, 61–84.
(20) Ehly, M.; Gemperline, P.; Nordon, A.; Littlejohn, D.; Basford, J. K.; De Cecco, M. *Anal. Chim. Acta* **2007**, *595*, 80–88.
(21) Gemperline, P.; Puxty, G.; Maeder, M.; Walker, D.; Tarczynski, F.; Bosserman, M. *Anal. Chem.* **2004**, *76*, 2575–2582.
(22) Puxty, G.; Fischer, U.; Jecklin, M.; Hungerbühler, K. *Chimia* **2006**, *60*, 605–610.

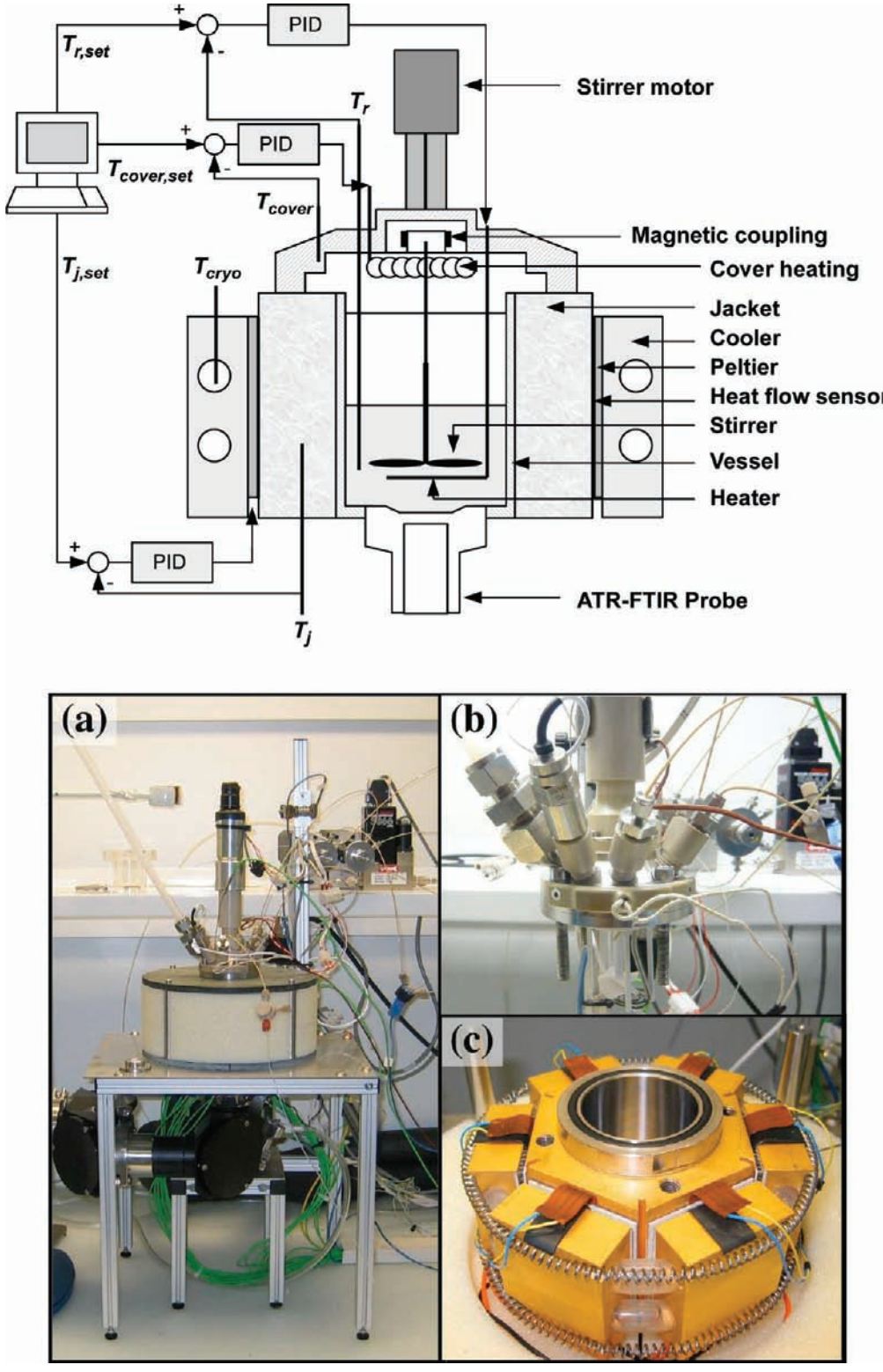

Figure 1. **(Top) Schematic of the combined reaction calorimeter, CRC.v5, with independent PID control of T_r, T_j, and T_{cover}. (Bottom) Images of (a) the calorimeter CRC.v5, (b) the electrically heated cover allowing for eight inserts, and (c) the copper jacket with the cooling system.**

and development in fine and pharmaceutical chemical industry where only small amounts of test substances are available. Despite the small volume of the reaction vessel, an attenuated total reflection Fourier transform infrared (ATR-FTIR) DiComp probe (Mettler-Toledo) is mounted directly at its bottom. A magnetically coupled pitched blade turbine with speeds up to 2000 rpm is used for stirring. The maximum pressure and temperature are up to 60 bar and about 200 °C, respectively. Instrumental control and data acquisition are operated with the Labview software, version 8.5, at a sampling rate of 10 Hz running on a 3.40 GHz Pentium 4 personal computer. The working principle of the calorimeter combines the compensation heater and heat balance principles. For details, we refer to Zogg et al.[23]

Table 1. **Experimental conditions for the semi-batch esterification of *n*-butanol (BuOH) by acetic anhydride (AA), catalysed by 1,1,3,3-tetramethylguanidine (TMG) under non-isothermal conditions**

initial reactor temperature, $T_{r,0}$	30 °C
initial jacket temperature, $T_{j,0}$	28 °C
initial cover temperature, $T_{cover,0}$	28 °C
ΔT_r, ΔT_j, ΔT_{cover}	50 °C
start of the ramp	10 min after starting the dosing
heating rate	1 °C/min
cryostat temperature, T_{cryo}	45 °C
initial reactor content	22 mL (0.233 mol) AA + 1.25 mL (10 mmol) TMG
dosing	21.4 mL (0.233 mol) BuOH
dosing rate, f_{dos}	3 mL/min
stirrer speed	500 rpm
pressure	atmospheric

The calorimeter used in this study is our latest version, the CRC.v5. Novelties of CRC.v5 compared to the previous version CRC.v4,[24] are (a) an electrical heater mounted directly into the cover, aiming at the diminution of heat loss and reducing the thermal inertia of the cover (a new system for thermostatting the cover, allowing also cooling, is under development and has been patented[25]), and (b) six heat flow sensors (Captec, France) located between the jacket and the Peltiers for measuring the heat flow due to cooling, $\dot{q}_{cool}$. (The expressions *heat flow sensor* and *heat flux sensor* are both present in literature. As we are interested in the flow [W] and not the flux [W/m^2], *heat flow* is preferred here.) The advantages of measuring $\dot{q}_{cool}$ with heat flow sensors instead of doing a heat balance over the Peltier elements, as performed previously,[23,24] are the following: (a) the temperature drop across the sensors is extremely reduced, (b) the real heat flow, $\dot{q}_{cool}$, is proportional to measured voltage and can be measured at real time, and (c) the sensitivity of the sensor, e.g. the proportionality constant between the heat flow and the measured voltage, is independent of the temperature.[26]

Data Treatment. The elucidation of the kinetic parameters and the reaction enthalpies requires first the determination of the power profile due to the reaction, $\dot{q}_{react}$. Three different methods for calculating $\dot{q}_{react}$ are used: *the global heat balance*, *the blank experiment*, and *the simulated blank*. Finally, the technique for optimising the kinetic parameters and the reaction enthalpies is explained.

Method 1: Evaluation with the Global Heat Balance. In reaction calorimetry, the classic method to determine the heat of reaction is to perform a global heat balance of the calorimeter,[7] as given in eq 1. For the notation, we refer to the list of symbols.

$$\dot{q}_{acc} = \dot{q}_{react} + \dot{q}_{comp} + \dot{q}_{mix} + \dot{q}_{stirr} + \dot{q}_{dos} - \dot{q}_{cool} - \dot{q}_{loss} \quad (1)$$

The power due to dosing, $\dot{q}_{dos}$ corresponding to the power required to bring the dosed material at the reactor temperature is given in eq 2, density, ρ_{dos} [kg/m^3], and heat capacity, $c_{p,dos}$ [J/(kg·K)], are taken from literature.[27]

$$\dot{q}_{dos} = f_{dos} \cdot \rho_{dos} \cdot c_{p,dos} \cdot (T_{dos} - T_r) \quad (2)$$

The power, $\dot{q}_{stirr}$, dissipated by the stirrer is negligible (<0.05 W). In the CRC.v5, the power due to cooling, $\dot{q}_{cool}$ is measured at real time by the six heat flow sensors covering each lateral side of the jacket.

The heat flow sensors do not cover the entire lateral surface of the jacket. Thus, a convective heat flow bypasses the heat flow sensors due to the temperature gradient between the jacket (T_j) and the coolers (T_{cryo}), see also Figure 1. When the temperature of the cover and the jacket are equal and the environmental temperature is constant (±0.5 °C), the heat loss, $\dot{q}_{loss}$, is expressed as a function of T_j and T_{cryo}, only:

$$\dot{q}_{loss} = a \cdot (T_j - T_{cryo}) + b \quad (3)$$

where the two temperature-independent parameters a [W/K] and b [W] are determined at steady-state directly before and after the reaction.

The heat accumulation is given by the sum of the individual heat capacities and corresponding temperature gradients at the various locations of the reactor, where the thermocouples are located. In our case, we consider only the temperature of the reactor, T_r, and of the jacket, T_j:

$$\dot{q}_{acc} = C_{p,r}\frac{dT_r}{dt} + C_{p,j}\frac{dT_j}{dt} \quad (4)$$

$C_{p,r}$ is the total heat capacity of the bulk [J/K], and $C_{p,j}$ is the total heat capacity of the calorimeter [J/K], including the jacket and the vessel, commonly called *calorimeter constant*. $C_{p,r}$ is calculated experimentally with temperature oscillation calorimetry,[28] and $C_{p,j}$ is calibrated from an experiment without chemical reaction, applying a temperature ramp. The derivatives of the temperatures were calculated employing a Savitzky−Golay filter,[29] with the following parameters: 121 data points, corresponding to 12.1 s of experiment, and a sixth-order polynomial fit.

Method 2: Evaluation with the Blank Experiment. With this method, the evaluation of the power due to the reaction, $\dot{q}_{react}$, requires to repeat the measurement with a reference. The assumption is that systematic errors are common to both reactive and reference experiments and therefore cancel out.[16] Here, as a reference, we dosed 21.4 mL of AA into 23.25 mL of AA. Assuming $\dot{q}_{dos}$, $\dot{q}_{loss}$, and $\dot{q}_{acc}$ cancel out in both experiments, $\dot{q}_{react}$ is determined by the difference between the measurement and the reference:

$$\dot{q}_{react} = \left(\dot{q}_{cool}^{meas} - \dot{q}_{cool}^{blank}\right) - \left(\dot{q}_{comp}^{meas} - \dot{q}_{comp}^{blank}\right) \quad (5)$$

where meas and blank are the reactive and blank (reference) experiments, respectively. Naturally, as the physical properties

(23) Zogg, A.; Fischer, U.; Hungerbühler, K. *Ind. Eng. Chem. Res.* **2003**, *42*, 767–776.
(24) Visentin, F.; Gianoli, S. I.; Zogg, A.; Kut, O. M.; Hungerbühler, K. *Org. Process Res. Dev.* **2004**, *8*, 725–737.
(25) Richner, G.; Wohlwend, M.; Neuhold, Y.-M.; Godany, T.; Hungerbühler, K. German Patent DE 102008020989 (A1), 2008.
(26) Richner, G. Dynamic study of a new small scale reaction calorimeter and its application to fast online heat capacity determination. Doctoral and Habilitation Thesis, Nr. 17972; Department of Chemistry, Swiss Federal Institute of Technology (ETH): Hönggerberg, Switzerland, 2008; DOI: 10.3929/ethz-a-005686831; http://dx.doi.org/10.3929/ethz-a-005686831.
(27) Yaws, C. *Chemical Properties Handbook*; McGraw-Hill: New York, 1999.
(28) Richner, G.; Neuhold, Y.-M.; Papadokonstantakis, S.; Hungerbühler, K. *Chem. Eng. Sci.* **2008**, *63*, 3755–3765.
(29) Maeder, M.; Neuhold, Y.-M. *Practical Data Analysis in Chemistry*; Elsevier: Amsterdam, 2007.

of the reference (AA dosed in AA) and those of the sample (BuOH dosed in AA:TMG) are different (e.g., at 30 °C, ρ_{AA} = 1071 g/L, ρ_{BuOH} = 802 g/L, $c_{p,\,AA}$ = 1.869 kJ/g, $c_{p,\,BuOH}$ = 2.170 kJ/g[27]), this induces an error in the determination of $\dot{q}_{react}$. This is an inevitable issue also known from investigations with twin reactor systems such as DSC and DRC.

Method 3: Evaluation with the Simulated Blank. The evaluation of the power due to the reaction, $\dot{q}_{react}$, by heat flow simulation of the blank is similar to method 2, but the reference is simulated by a dynamic heat flow model rather than being measured. The heat flow and temperature profiles through the reactor content, the vessel and the jacket are simulated for a preselected reactor content. More details are given in Appendix A and by Richner.[26] $\dot{q}_{react}$ is determined by the difference between the measurement and the simulated reference:

$$\dot{q}_{react} = \left(\dot{q}_{cool}^{meas} - \dot{q}_{cool}^{sim}\right) - \left(\dot{q}_{comp}^{meas} - \dot{q}_{comp}^{sim}\right) \qquad (6)$$

where meas and sim are the reactive (measured) and the simulated (reference) experiments. Partial volumes of the different components are assumed additive, i.e. a possible excess volume is not considered.

Kinetic Analysis. Zogg et al.[8] reviewed different evaluation techniques for the identification of reaction enthalpy and reaction model parameters under isothermal conditions from calorimetric measurements. With nonisothermal conditions, the similar techniques can be applied. For the simultaneous identification of the reaction enthalpy and the model parameters (rate constant and activation energy), we used a model-based evaluation, for which a reaction mechanism must be postulated. The reaction rate $r_i(k_i, t)$ for a reaction i is given by the set of ordinary differential equations (ODE) corresponding to the rate law, see also eq 11. The temperature dependence of the rate constant k_i is given by the Arrhenius equation, eq 7, where $k_{ref,i}$ is the rate constant at the reference temperature T_{ref}.

$$k_i = k_{ref,i}\, e^{-(E_{a,i}/R)(1/T - 1/T_{ref})} \qquad (7)$$

For the respective number of reactions N_r, the reaction enthalpies, $\Delta_r H_{1...N_r}$, the activation energies $E_{a,1...N_r}$ and the reference rate constant, $k_{ref,1...N_r}$, are determined for the experimental calorimetric data using Matlab's nonlinear least-squares curve-fitting tool, *lsqcurvefit*, with eq 8 as the objective function.

$$\min_{k_{ref,1...N_r},\Delta_r H_{1...N_r},E_{a,1...N_r}} \left\{ \left[\dot{q}_{react} - V_r \sum_{i=1}^{N_r} r_i(-\Delta_r H_i) \right]^2 \right\} \qquad (8)$$

Additionally, we determined the total process enthalpy, ΔH, that includes reaction enthalpy and heat of mixing, by a simple model-free evaluation technique that consists of directly integrating $\dot{q}_{react}$.

Results and discussion

Temperature Control. Figure 2a shows the temperatures of the reactor, the jacket, and the cover during the course of the esterification under nonisothermal conditions. The temperature deviations from the set points are below 0.2 °C for T_r and T_j and 0.4 °C for T_{cover}. In all cases, the maximum deviation appears directly after the start and the end of the ramp while during the ramp the deviations are within the noise level (0.03 °C for T_r, 0.01 °C for T_j and 0.04 °C for T_{cover}). The compensation heater provides a fast control of the reactor temperature, and the powerful cooling system allows an ideal control of the jacket temperature. In comparison, under isothermal conditions at 40 °C in commercially available 75 mL and 5 L reactors, the reactor temperature deviates above the set point up to 13 and 40 °C, respectively.[20]

This demonstrates that the CRC.v5 provides a well controlled environment also when working under nonisothermal conditions. The corresponding powers of the compensation heater and of the cooling are shown in Figure 2b.

Heat of Reaction. In the next sections, we assess the three different methods for the determination of $\dot{q}_{react}$, and the issues regarding possible change of the global heat transfer, the heat loss, and the heat accumulation during the reaction.

Global Heat Transfer. In the CRC.v5, the power due to cooling, $\dot{q}_{cool}$, is measured online via heat flow sensors, without calibration of the global heat transfer, *UA*. In contrast, in their nonisothermal kinetic study with RC1, Hoffmann et al.[11] calibrated *UA* before and after the reaction, interpolated the values in between, and performed about 20 additional calibrations of *UA* to validate the interpolation. In the CRC.v5, due to the calibration-free measurement of the cooling power, the possible changes of *UA* would not be an issue for method 1 (global heat balance). In method 2 (blank experiment), a change of *UA* during the reaction would deviate from the reference measurement. For such a case, a second reference with the products should be measured.[16] The drawback is indubitably the increased number of experiments per investigation, which may not even be feasible if, e.g., the phase of the product changes within the temperature range. Finally, with method 3, the possible change of *UA* during the course of the reaction is already accounted for by the heat flow model. The internal heat transfer coefficient is a model parameter that is reoptimised during the course of the experiment. Further details are given in Appendix A.

Heat Loss. Solvent vaporisation and condensation in the vessel are known to contribute to the total heat loss and consequently shift the baseline of the heat signal. In this case, heat loss is often evaluated by trial and error adjustment of the baseline.[30] According to Henry's law, the mass fraction of solvent in the gas phase should decrease with increasing reactor pressure. In the CRC.v5, 25 mL of water at 75 °C have been pressurised from 1 to 45 bar resulting in a decrease of heat loss from 2.99 to 2.98 W, only. Consequently, we neglect vaporisation/condensation effects and heat loss can be calibrated as a function of the apparatus only, independently of the reactor content. Due to the fast temperature control of the cover, the heat loss can be calculated as a function of the jacket and cryostat temperatures only (assuming a constant temperature of the environment during the course of the reaction, in our case, ±0.5 °C), and thus be determined by a proportional correlation.

Heat Accumulation. In small-scale reactors, the heat accumulated by embedded probes may represent a large contribution

(30) Ubrich, O.; Srinivasan, B.; Lerena, P.; Bonvin, D.; Stoessel, F. *Chem. Eng. Sci.* **2001**, *56*, 5147–5156.

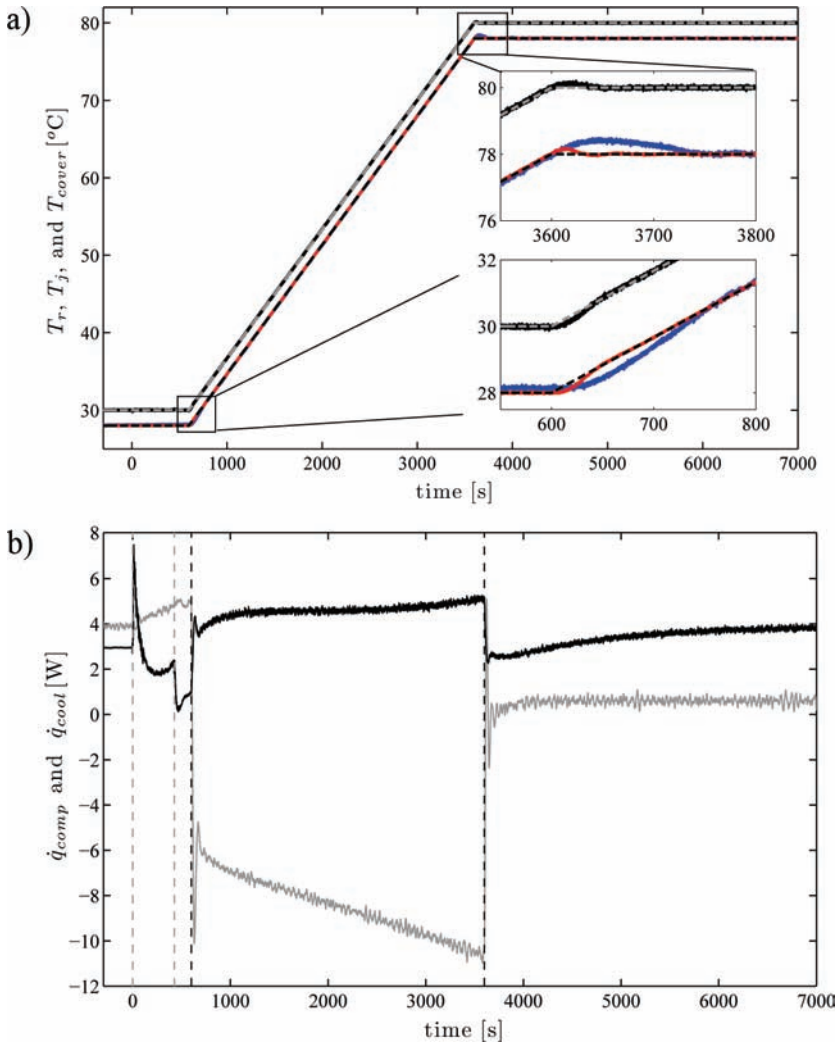

Figure 2. **Temperature and power during the esterification of BuOH and AA catalysed by TMG under nonisothermal conditions. (a) Measured temperatures of the reactor, T_r (black line), the jacket, T_j (red line), and the cover, T_{cover} (blue line). The dashed lines represent the corresponding set-point temperatures. (b) Power of the compensation heater (black) and of the cooling (grey). The vertical dashed grey and black lines represent the start and the end of the dosing and of the temperature ramp, respectively. The experimental conditions are given in Table 1.**

of the total heat accumulated by the system. We investigated the effect of the bottom mounted IR-probe on the baseline by measuring two references, with and without IR-probe. Figure 3 shows the resulting $\dot{q}_{comp}$ and $\dot{q}_{cool}$. We can observe peaks at the beginning and the end of the temperature ramp (at 800 s and 3800 s). We may distinguish the narrow and the broad peaks with a width of 50 s and ~400 s, respectively.

The narrow peaks are due to the dynamics of the calorimeter, that is of major importance for the deviations from the set point temperatures.[8] The dynamics should be fast to accurately control the temperature of the reaction medium as discussed above. The compensation heater and the cooling system have time constants of 4 s and 15 s, respectively,[24] which is more than 10 times faster than in standard reaction calorimeters.[8] The drawback is a strong peak of the power at the beginning and the end of the temperature ramp. With methods 2 and 3, the dynamics are taken into account by the blank measurement and the heat flow modelling, respectively. Thus, both methods allow for compensating the dynamics. Method 1 does not account for the dynamics at all, and consequently shows the highest peaks (see Figure 4).

The broad peaks (width ~400s) are due to heat accumulation in thermally noncontrolled parts of the system. As shown in Figure 3, these peaks are not observed on $\dot{q}_{comp}$ for the measurement without the IR-probe while $\dot{q}_{cool}$ from both cases perfectly superimposed. We can conclude that (a) the major contribution to the broad peaks comes from the IR-probe and (b) $\dot{q}_{cool}$ is not affected by the IR-probe. The difference of $\dot{q}_{comp}$ is about 1.3 W that corresponds to a heat capacity of 80 W/K. In method 1, few calibrations would be required to account for this effect. With commercial calorimeters, this is usually performed by the manufacturer and hidden in the control software. Method 2 accounts perfectly for it, while for method 3, the shape of the IR-probe is too complex to be accurately modelled within our heat flow model. Simulation with commercial finite element software such as FemLab or Ansys could provide more accurate results but the simulation of an entire reaction would require extensive computational time and, thus, cannot be used on an everyday basis. One could expect that the heat accumulation in the cover would contribute to a significant shift of the baseline. However, due to the well

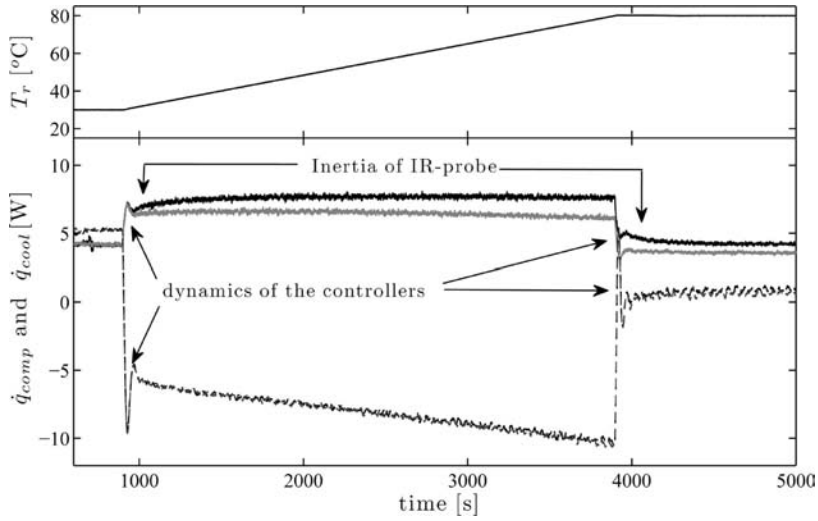

Figure 3. **Effect of the IR bottom-mounted probe on the calorimeter dynamics during a temperature ramp of 1 °C/min with 44.7 mL of AA as reactor content. Power of the compensation heater, $\dot{q}_{comp}$, (full lines) and heat of cooling, $\dot{q}_{cool}$, (dashed lines) with and without IR-probe (black and grey lines, respectively).**

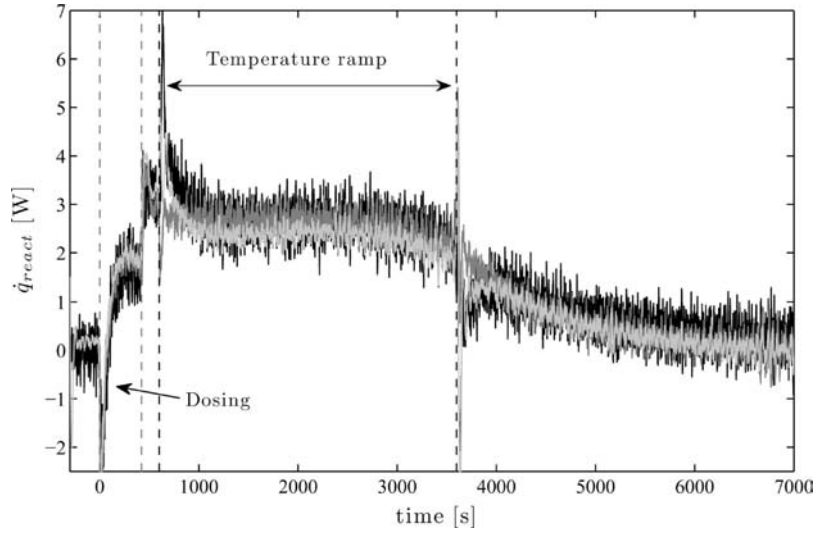

Figure 4. **Reaction power, $\dot{q}_{react}$ during the esterification of BuOH and AA catalysed by TMG under nonisothermal conditions, with $\dot{q}_{react}$ determined by: method 1 (global heat balance, black), eq 1, method 2 (blank experiment, dark grey), eq 5, and method 3 (simulated blank, light grey), eq 6. The vertical grey and black lines represent the periods of dosing and of the temperature ramp, respectively. The experimental conditions are given in Table 1.**

controlled temperature of the cover (see Figure 2), this cannot be observed with the CRC.v5.

The power of the reaction, $\dot{q}_{react}$, determined from the three different methods is shown in Figure 4. The deviations between the three methods are observed only after the start and the end of the temperature ramp for the reasons explained above. The noise level that comes principally from the calculation of the derivatives of the reactor and jacket temperatures is higher for method 1 (0.28 W). The simulated reference is free of noise; thus, the noise level with method 3 (0.15 W) is lower than that with method 2 (0.22 W).

Kinetics and Reaction Mechanism. During the dosing, the profile of $\dot{q}_{react}$ shows an endothermic heat effect in addition to the heat released by the esterification reaction. This endothermic effect was already observed[20] and can, for example, be explained by a shift of the equilibrium from the activated catalyst complex towards its dissociated components during the dosing (i.e., volume change), or more complex solvation effects. The mixing of TMG into AA liberates -0.85 ± 0.05 kJ/mol of TMG (not shown here). The addition of BuOH into AA absorbed also 5.28 ± 0.10 kJ/mol of BuOH as shown later in Figure 7. Thus, the dosing of BuOH into the TMG:AA mixture might follow a complex equilibrium mechanism. The investigation of such phenomena was not the scope of this study and not further pursued. For the optimisation of the kinetic parameters, the calorimetric measurements during the dosing period were not considered.

For the model-based evaluation we first postulated the esterification to be a pseudo-second-order reaction mechanism with a steady-state assumption on the TMG concentration after dosing, similarly to Puxty et al.[31] The optimised kinetic parameters obtained from the three different methods for the heat balance are given in Table 2. Figure 5 shows $\dot{q}_{react}$

(31) Puxty, G.; Neuhold, Y.-M.; Ehly, M.; Jecklin, M.; Gemperline, P.; Nordon, A.; Littlejohn, D.; Basford, J. K.; De Cecco, M.; Hungerbühler, K. *Chem. Eng. Sci.* **2008**, *63*, 4800–4809.

Table 2. **Overview of the kinetic parameters and reaction enthalpy for the esterification of *n*-butanol with and without TMG for different reaction mechanisms and three evaluation methods of $\dot{q}_{react}$[a]**

model		experiment	ΔH^b [kJ/mol]	$\Delta_r H^c$ [kJ/mol]	$k_{ref,1}$ [M^{-2} s^{-1}]	$E_{a,1}$ [kJ/mol]	$k_{ref,2}$ [M^{-2} s^{-1}]	$E_{a,2}$ [kJ/mol]
		With TMG						
catalytic	eq 9	method 1	-54.4 ± 2.6	-64.0 ± 2.8	$3.2 \pm 0.2 \times 10^{-4}$	27.4 ± 0.7	–	–
		method 2	-48.8 ± 3.6	-59.4 ± 3.3	$2.8 \pm 0.2 \times 10^{-4}$	34.3 ± 1.6	–	–
		method 3	-48.3 ± 1.6	-59.5 ± 2.1	$3.4 \pm 0.2 \times 10^{-4}$	31.0 ± 2.4	–	–
		With TMG						
parallel	eqs 9 and 10	method 1	-54.4 ± 2.6	-57.1 ± 3.7	$3.2 \pm 0.6 \times 10^{-4}$	15.7 ± 5.8	$1.4 \pm 0.4 \times 10^{-5}$	84 ± 16
		method 2	-48.8 ± 3.6	-55.4 ± 3.4	$2.7 \pm 0.4 \times 10^{-4}$	18.2 ± 4.9	$1.0 \pm 0.4 \times 10^{-5}$	87 ± 12
		method 3	-48.3 ± 1.6	-54.4 ± 1.4	$3.4 \pm 0.1 \times 10^{-4}$	13.6 ± 4.7	$1.7 \pm 0.6 \times 10^{-5}$	88 ± 8
		Without TMG						
noncatalytic	eq 10	method 1	-47.7 ± 2.0	-67.3 ± 1.0	–	–	$3.2 \pm 0.1 \times 10^{-6}$	84 ± 0.4
		method 2[d]	-48.6	-69.2	–	–	2.6×10^{-6}	91.2
		method 3	-47.7 ± 1.1	-67.0 ± 1.4	–	–	$3.6 \pm 0.4 \times 10^{-6}$	83.5 ± 2.0
		With TMG						
literature	eq 9	Puxty et al.[22]	–	-43^{+3}_{-8}	$4.0 \pm 1 \times 10^{-4}$	37.3 ± 0.01	–	–
		Puxty et al.[31]	–	–	5×10^{-4}	30[e]	–	–
		Puxty et al.[31]	–	–	6×10^{-4}	31[e]	–	–

[a] Method 1: *global heat balance*. Method 2: *blank experiment*. Method 3: *simulated blank*. Errors for this study are given in one standard deviation based on three replicates; see text and given references for more details on errors. $T_{ref} = 40$°C. [b] ΔH is given by the integral of $\dot{q}_{react}$, and thus includes also the heat of mixing. [c] $\Delta_r H$ is the heat of reaction obtained from optimisation excluding the dosing period, and thus does not include the heat of mixing. [d] One single experiment. [e] Measurement based on near-IR spectroscopy.

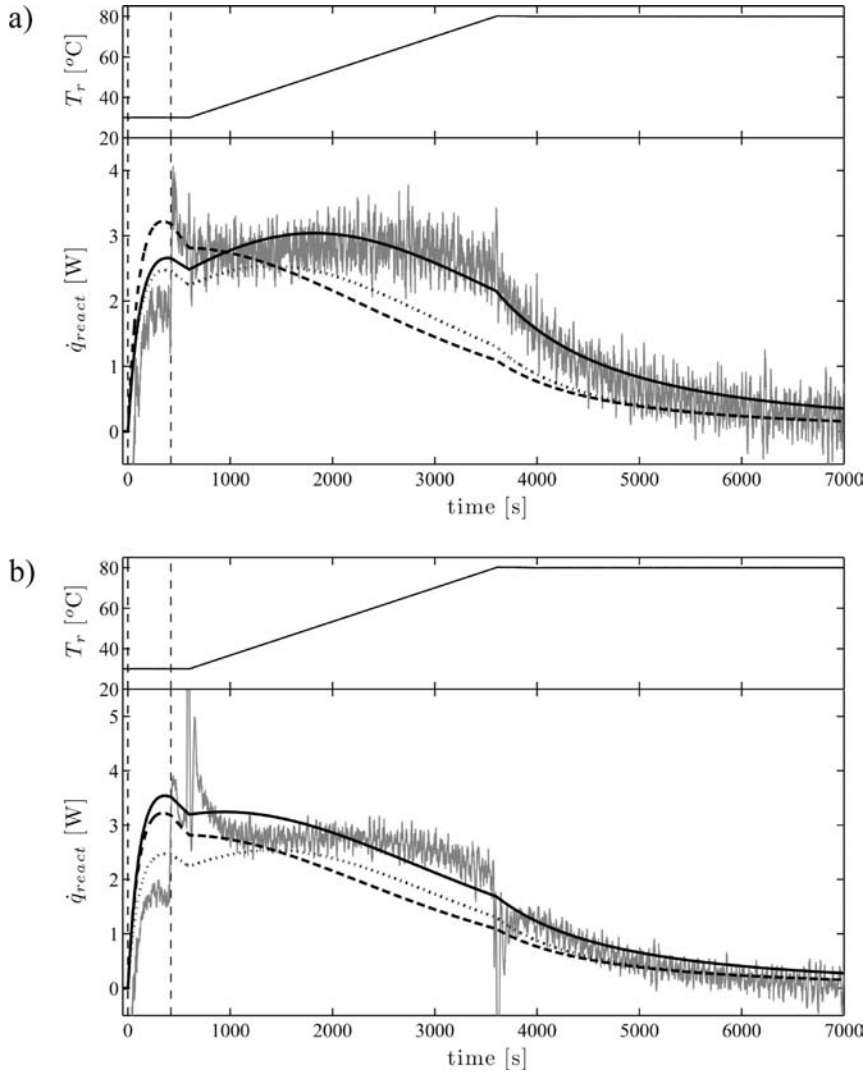

Figure 5. **Modelled and measured power of the reaction, $\dot{q}_{react}$, during the esterification of BuOH and AA catalysed by TMG under nonisothermal conditions. The measured data (full grey line) are determined with methods 2 (a) and 3 (b), the modelled data are given for a pseudo-second-order catalytic mechanism with the optimised parameters determined in this study (full black line), and from literature (black dotted line,[22] black dashed line,[31] with $\Delta_r H = -43$ kJ/mol, see Table 2). The experimental conditions are given in Table 1.**

determined with methods 2 and 3, and the resulting simulation. For comparison, simulations with published kinetic parameters[31] are also shown. Apparently, none of the simulations fits the measurement reasonably. This is particularly the case for the relatively flat power profile between 600 and 3000 s corresponding to the temperature ramp.

Autocatalytic behaviour is frequently observed during esterification between anhydrides and alcohols,[18] due to the formation of organic acid. However, as TMG is a strong base, the acid activity is assumed to be low, and no autocatalysis is expected. Here, we propose that a base-catalysed and an uncatalysed reaction path take place simultaneously, following a parallel mechanism of pseudo-second-order (with constant C_{TMG} after dosing) and second-order rate laws, respectively.

$$\mathbf{BuOH} + \mathbf{AA} + \mathbf{TMG} \xrightarrow{k_1} \mathbf{BuOA} + \mathbf{AH} + \mathbf{TMG} \quad (9)$$

$$\mathbf{BuOH} + \mathbf{AA} \xrightarrow{k_2} \mathbf{BuOA} + \mathbf{AH} \quad (10)$$

The resulting ordinary differential equations (ODEs) are given in eq 11.

$$\begin{cases} \frac{dC_{BuOH}}{dt} = -r_1(k_1,t) - r_2(k_2,t) + \frac{f_{dos}}{V_r(t)} \cdot (C_{dos,BuOH} - C_{BuOH}(t)) \\ \frac{dC_{AA}}{dt} = -r_1(k_1,t) - r_2(k_2,t) - \frac{f_{dos}}{V_r(t)} \cdot C_{AA}(t) \\ \frac{dC_{BuOA}}{dt} = r_1(k_1,t) + r_2(k_2,t) - \frac{f_{dos}}{V_r(t)} \cdot C_{BuOA}(t) \\ \frac{dC_{AH}}{dt} = r_1(k_1,t) + r_2(k_2,t) - \frac{f_{dos}}{V_r(t)} \cdot C_{AH}(t) \\ \frac{dC_{TMG}}{dt} = -\frac{f_{dos}}{V_r(t)} \cdot C_{TMG}(t) \\ \frac{dV_r}{dt} = f_{dos} \\ r_1(k_1,t) = k_1 \cdot C_{BuOH}(t) \cdot C_{AA}(t) \cdot C_{TMG}(t) \\ r_2(k_2,t) = k_2 \cdot C_{BuOH}(t) \cdot C_{AA}(t) \\ k_1 = k_{ref,1} \cdot e^{-(E_{a,1}/R)(1/T - 1/T_{ref})} \\ k_2 = k_{ref,2} \cdot e^{-(E_{a,2}/R)(1/T - 1/T_{ref})} \end{cases} \quad (11)$$

To show that within this temperature range the uncatalysed reaction already is competing, we investigated the reaction under the conditions given in Table 1 but without the catalyst. Figure 7 shows the resulting fits for $\dot{q}_{react}$ calculated with methods 2 and 3.

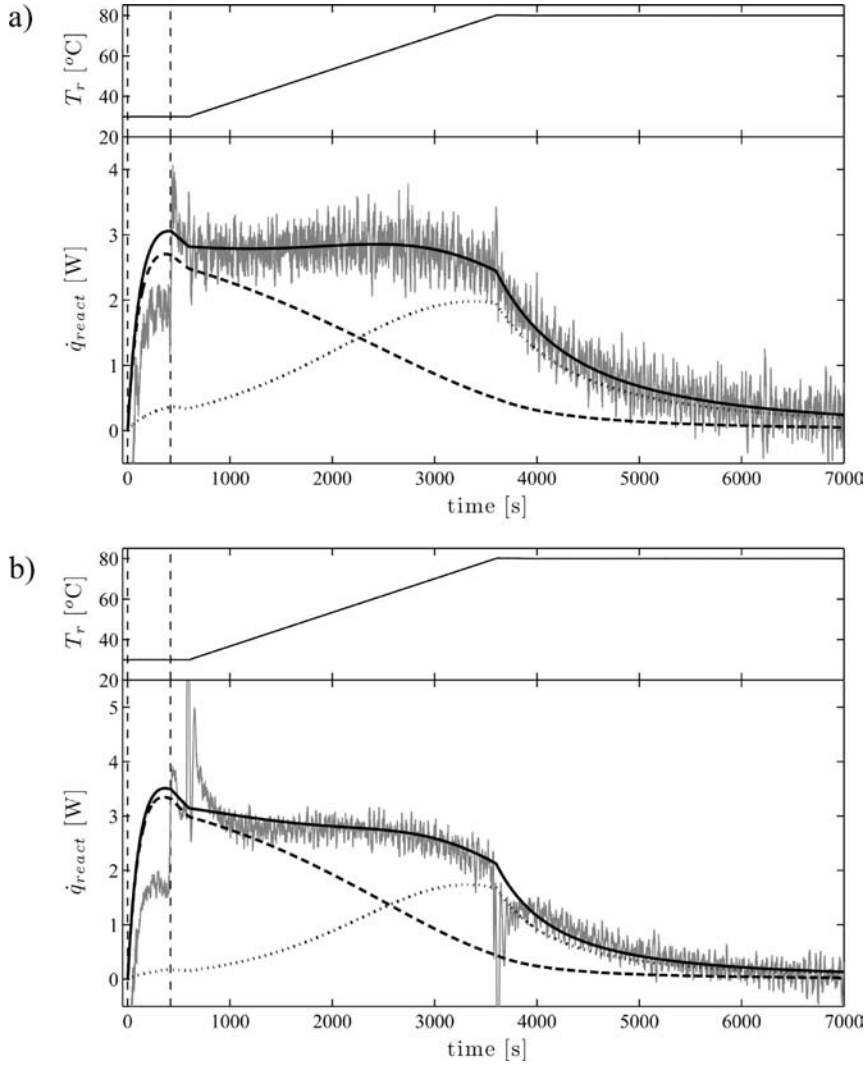

Figure 6. **Fitted (black line) and measured (grey line) reaction power, $\dot{q}_{react}$, during the esterification of BuOH and AA catalysed by TMG under nonisothermal conditions. The kinetic model includes both a catalytic and noncatalytic reaction step. The contributions to $\dot{q}_{react}$ of both reaction steps are given by the dashed and dotted lines, respectively. $\dot{q}_{react}$ is determined with methods 2 (a) and 3 (b). The reaction conditions are given in Table 1.**

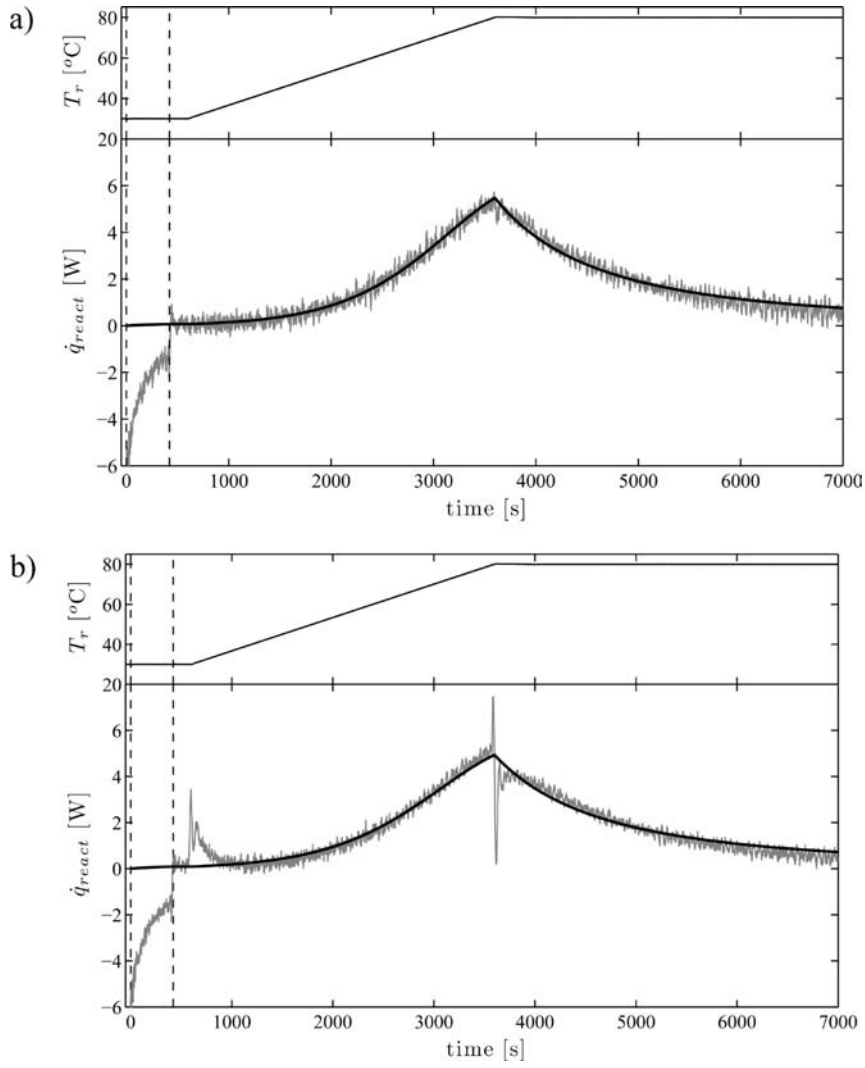

Figure 7. **Fitted (black line) and measured (grey line) reaction power, $\dot{q}_{react}$, for the esterification of BuOH and AA without catalyst under nonisothermal conditions. The kinetic model is comprised by the noncatalytic reaction step only. $\dot{q}_{react}$ is determined with methods 2 (a) and 3 (b). The reaction conditions are given in Table 1.**

Obviously, the reaction "starts" after 1600 s at about 45 °C, which may explain that the uncatalysed reaction was not observed in the published studies only covering a temperature range of 30−50 °C. The endothermic peak before 500 s is due to the heat of mixing of BuOH into AA. The second peak at 900 s (start of the temperature ramp) is due to the dynamics of the calorimeter as already discussed above. Activation energy and reaction enthalpy (see Table 2) correspond well to the data published by Widell and Karlsson,[18] who used methanol instead of *n*-butanol (E_a = 68.1 kJ/mol and $\Delta_r H$ = −67.1 kJ/mol). In this particular case, as TMG is not present, autocatalytic behaviour may also occur. However, considering the good quality of the fit, including an additional step would not be reasonable.

Finally, the kinetic parameters for the two parallel reactions, eqs 9 and 10 have been simultaneously optimised for the calorimetric measurements with TMG used as catalyst. As the reaction enthalpy, $\Delta_r H$, is a state function, i.e. depending only on the initial and final states of the system, $\Delta_r H$ is assumed to be the same for both reaction steps. The resulting parameters are given in Table 2 and illustrated in Figure 6 for methods 2 and 3. Obviously, the additional contribution of the uncatalysed reaction, shown as the dotted line in Figure 6, allows to explain the profile of $\dot{q}_{react}$. The quality of the fit, given by the sum of the residuals, is improved by about 25% with the parallel reaction steps compared to the fit with the catalysed reaction step only. The activation energy of the uncatalysed reaction, optimised for the data with and without TMG, are equal within the error limits. E_a and k_{ref} of the catalysed reaction are 25% and 50% below the values given in literature.[31] However, Figure 4 in Puxty's publication[31] (3D contour plots of the response surfaces) does show a high ambiguity (valley shape) regarding the minimum of the objective function for the determination of the kinetic parameters.

Theoretically, from one single nonisothermal measurement, the simultaneous evaluation of the model parameters of two parallel reactions results in two different sets of optimal parameters (e.g., two local minima of the objective function eq 8, with N_r = 2). Complementary information such as an additional measurement under different conditions or analysis with chromatographic techniques is necessary. Here, we assumed that the catalysed reaction is faster than the uncatalysed one, and thus, we set the parameter constraints in the objective function accordingly. With all three methods, the constraint lower and upper bounds were $\Delta_r H$: −100 to −1 kJ/mol, $k_{ref,1}$: 10^{-6} to 0.1 m^{-2} s^{-1}, $E_{a,1}$: 1−100 kJ/mol, $k_{ref,2}$: 10^{-8} to 3 × 10^{-5} m^{-2} s^{-1}, and $E_{a,2}$: 50−100 kJ/mol. Any initial estimates within these boundaries converged to the same optimised parameters.

The errors in Table 2 are calculated by the standard deviation of the optimised values, based on three replicates of the

experiment. Note that the errors given for the corresponding literature values[22] based on a second-order global analysis tend to be unreasonably small due to possible nonrandom contributions between the individual experiments and too large a degree of freedom.[32] Thus, the errors from both studies are not straightforwardly comparable. Surprisingly, despite the simultaneous optimisation of five parameters to a monovariate measurement, the variance/covariance matrix[29] did not show strong correlations between the five parameters. We can observe that the activation energy of the catalysed reaction, $E_{a,1}$ and the rate constant of the uncatalysed reaction, $k_{ref,2}$ have a high error (about 30%). However, the difference between the simulated reaction powers is below the noise level of a measurement. For comparison, in his publication on nonisothermal calorimetry, Hoffmann et al.[11] also gave an error of 50% on the preexponential factor of a second order reaction.

Conclusions

The reaction calorimeter, CRC.v5, combines the principles of power compensation and heat balance. For the first time, the performance of the CRC.v5 was demonstrated under nonisothermal conditions. Usually, it is a challenging task to account for possible baseline shift due to temperature modulation without extensive time-consuming calibration. The CRC.v5 allows for an independent control of the reaction, the jacket, and the cover temperatures. The heat of cooling is measured at real time with heat flow sensors, and thus does not require calibration of the global heat transfer coefficient.

We applied three different methods for the determination of the reaction power employing either a global heat balance, a measured reference or, as a novelty, a simulated reference. A rigourous dynamic heat flow model of the calorimeter allows the simulation of a reference measurement rather than measuring it, thus saving a considerable amount of experimental time. The shifts due to the reactor dynamics and the heat accumulation of the system are not equally accounted for in all three methods of heat balancing. The choice of one method depends on the reaction and operating conditions. Reaction time, heating rate, and reactor dynamics are three important factors to consider. For example, if the reaction time is faster than the dynamics, method 2 should be preferred. If large changes of physical properties of the reaction mixture are expected, method 3 should be used. For other cases, method 1 could provide enough accuracy. In our case study, only minor differences in the kinetic parameters and reaction enthalpies have been observed. Obviously, the good thermal dynamics of our reactor does not favor one of the methods for heat balancing. The results of the experiments indicate that the solvent-free base-catalysed esterification of *n*-butanol by acetic anhydride follows a mechanism of two competitive parallel catalytic and noncatalytic steps. The reaction enthalpy and the model parameters (rate constant and activation energy) of both reactions could be simultaneously evaluated from one single nonisothermal calorimetric measurement using a model-based evaluation method, under the assumption that the activation energy is lower for the catalysed reaction than for the uncatalysed reaction.

Method 3 requires preceding experimental work to determine the parameters for the heat flow model. In comparison, with commercial reaction calorimeters, the dynamics is empirically corrected by numerous calibrations (performed generally by the manufacturer). From the scientific point of view, we consider a physically meaningful model superior to an empirical calibration due to an intrinsic understanding. This technique could easily be adapted and implemented into commercial calorimeters capable of measuring the heat of cooling at real time, e.g. via heat flow sensors.

Model-based kinetic analysis of a single nonisothermal experiment should be done with caution to avoid erroneous or rather naive interpretations. Reasons for this can be due to the experimental setup (e.g., inefficient stirring) but also due to the mechanistic model that may lead to inevitable ambiguities in the kinetic parameters. For this study, the well-stirred vessel allowed us to exclude mass transfer effects. A reasonable assumption in the form of a simple and validated constraint broke the mathematical ambiguity.

List of Symbols and Definitions

Table 3. **List of symbols and definitions**

symbol	unit	description
A	m^2	heat exchange area
a	W/K	calibration parameter of the heat loss
b	W	calibration parameter of the heat loss
C_{AA}	M	concentration of acetic anhydride
C_{BuOA}	M	concentration of butyl acetate
C_{AH}	M	concentration of acetic acid
C_{BuOH}	M	concentration of *n*-butanol
C_{TMG}	M	concentration of 1,1,3,3-tetramethylguanidine
$C_{p,r}$	J/K	total heat capacity of the reactor content
$C_{p,j}$	J/K	total heat capacity of the jacket
$c_{p,dos}$	J/(kg·K)	heat capacity of the dosing
e	K	error between actual and set temperature values
$E_{a,i}$	kJ/mol	activation energy of the *i*th reaction
k_i	$(L/mol)^{n-1}/s$	rate constant of the *i*th reaction of *n*th order
$k_{ref,i}$	$(L/mol)^{n-1}/s$	rate constant of the *i*th reaction of *n*th order at T_{ref}
K	W/K	gain of the controller
h_{bottom}	W/(m²·K)	heat transfer coefficient of the heat loss at the bottom of the vessel
h_r	W/(m²·K)	internal heat transfer coefficient (reactor side)
h_{side}	W/(m²·K)	heat transfer coefficient of the heat loss from the jacket to the coolers
h_{top}	W/(m²·K)	heat transfer coefficient of the heat loss from the jacket to the cover
ΔH	J/mol	process enthalpy
$\Delta_r H_i$	J/mol	reaction enthalpy of the *i*th reaction
f_{dos}	mL/min	dosing rate
N_r	–	number of reactions
$\dot{q}_{acc}$	W	heat accumulation
$\dot{q}_{comp}$	W	power of the compensation heater
$\dot{q}_{cool}$	W	heat flow of the cooling
$\dot{q}_{dos}$	W	heat flow of dosing
$\dot{q}_{mix}$	W	heat due to mixing
$\dot{q}_{loss}$	W	heat flow lost to the environment
$\dot{q}_{PID}$	W	simulated power calculated by the PID controller
$\dot{q}_{phase}$	W	heat flow due to phase change
$\dot{q}_{react}$	W	heat produced by the reaction
$\dot{q}_{stirr}$	W	power due to the stirrer
$\dot{q}_{V,ext}$	W/m³	density of heat from an external source
r	m	radial coordinate
r_i	mol/(L·s)	reaction rate of the *i*th reaction
t	s	time
T	K or °C	temperature
T_{cryo}	K or °C	temperature of the cryostat and of the coolers
T_{dos}	K or °C	temperature of the dosing
T_{env}	K or °C	temperature of the environment
T_j	K or °C	temperature of the jacket
T_r	K or °C	temperature of the reactor content
$T_{r,set}$	K or °C	set-point temperature of the reactor content
U	W/(m²·K)	heat transfer coefficient
V_r	L or m³	volume of the reactor content
z	m	Cartesian coordinate
λ	W/(m·K)	thermal conductivity
ρ	kg/m³	fluid density
τ_D	s	derivative time of the PID
τ_I	s	integral time of the PID
$\tau_{q_{comp}}$	s	time constant of the compensation heater
ϕ	rad	angular coordinate
ϕ_{T_r}	s	dead time of the reactor temperature measurement
blank		blank measurement
dos		dosing
meas		measurement
sim		simulation
0		initial value

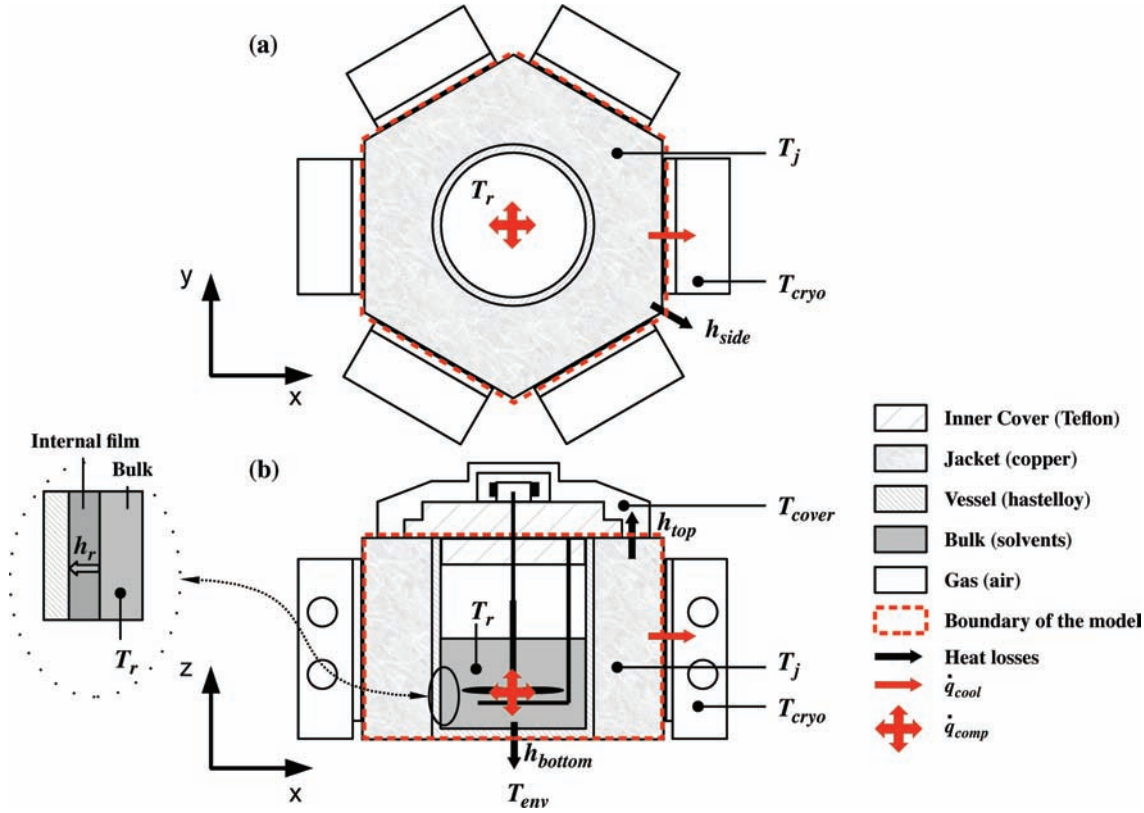

Figure A-1. **Illustration of the boundary conditions for the heat flow model of the CRC.v5. (a) top view (b) side view. Note that both the cover and the bottom mounted IR-probe (not shown here) are outside the boundaries of the model.**

Appendix A

Modelling with Finite Difference Method. The temperature and heat flow profiles through a solid body due to thermal conduction are governed by Fourier's law. In cylindrical coordinates, it is given by:

$$\frac{\delta T(\phi,r,z,t)}{\delta t} = \frac{\lambda}{\rho c_p}\left[\frac{\delta}{r\delta r}\left(r\frac{\delta T}{\delta r}\right) + \frac{\delta}{r^2\delta\phi}\left(\frac{\delta T}{\delta\phi}\right) + \frac{\delta}{\delta z}\left(\frac{\delta T}{\delta z}\right) + \frac{\dot{q}_{V,\text{ext}}}{\lambda}\right] \tag{A-1}$$

The finite difference model used in method 3 was based on the discretized form of eq A-1. This equation was discretized along the spatial variables r and z while we assumed a symmetry along the radial axis (e.g., $(\delta T)/(\delta\phi) = 0$). An optimal discretization considered 273 elements, leading to 273 ODEs that were solved in Matlab.

In eq A-1, $\dot{q}_{V,\text{ext}}$ represents the external heat sources, such as the heat loss, the power of cooling and the compensation power. The boundaries of the model are illustrated in Figure A-1. h_{top}, h_{bottom} and h_{side} are three different heat loss coefficients that were characterised by a set of experiments at steady-state where T_r, T_j, T_{cover}, and T_{cryo} were alternately changed. The internal heat transfer coefficient, h_r is determined by an optimisation procedure performed with Matlab's single-variable optimiser, *fminbnd*, over a fixed interval, given by eq A-2.

$$\min_{h_r}\{[\dot{q}_{comp}^{sim} - \dot{q}_{comp}^{meas}]^2\} \tag{A-2}$$

The material properties (thermal conductivity, λ, density, ρ, and heat capacity, c_p) were taken from literature[33] for copper (jacket) and air (gas phase of the reactor), and from the producer [Haynes International] for Hastelloy (vessel). The heat capacity of the bulk, $C_{p,r}$ was determined experimentally by temperature oscillations. The advantages are the following: (a) with temperature oscillation, even during the course of a reaction, the heat capacity can be determined, and (b) heat capacity of the inserts (embedded probes), the stirrer, the optional baffles, and the heater are accounted for. For details on temperature oscillation calorimetry, we refer to Richner et al.[28] As the mass of reactants is known and the vessel content is assumed to be perfectly mixed, λ and ρ of the bulk are not required.

The modelling of $\dot{q}_{comp}$ and $\dot{q}_{cool}$ includes the dynamics of the calorimeter, characterised by the PID settings of the thermal regulator, and the time constant and dead time of the thermocouples. The PID controller modelling for $\dot{q}_{comp}$ involves the three separate parameters given by:

$$\dot{q}_{comp}^{PID}(t) = K\left[e(t) + \frac{1}{\tau_I}\cdot\int_0^t e(t')dt' + \tau_D\cdot\frac{\delta e(t)}{\delta t}\right] \tag{A-3}$$

with

$$e(t) = T_{r,set} - T_r(t - \phi_{T_r}) \tag{A-4}$$

K, τ_I, and τ_D are the gain [W/K], the integral time [s], and the derivative time [s], respectively. ϕ is the dead time of the sensor.

The time constant characterises the dynamic response of a sensor or, more generally, of a system. The theoretical response $A(t)$ to a signal step ΔA of a linear system of first order is $A(t) = A_0 + \Delta A[1 - \exp(-t/\tau)]$. Thus, combining the PID control,

eq A-3, the dead time, eq A-4, and the time constant, τ, gives:

$$\dot{q}^{\mathrm{sim}}_{\mathrm{comp}}(t) = \dot{q}^{\mathrm{sim}}_{\mathrm{comp}}(t-1) + [\dot{q}^{\mathrm{PID}}_{\mathrm{comp}}(t) - \dot{q}^{\mathrm{sim}}_{\mathrm{comp}}(t-1)] \times [1 - \mathrm{e}^{-t/\tau_{q_{\mathrm{comp}}}}] \quad \text{(A-5)}$$

where $\dot{q}^{\mathrm{sim}}_{\mathrm{comp}}$ is the simulated value of the compensation heater, $\dot{q}^{\mathrm{PID}}_{\mathrm{comp}}$ the target value given by eq A-3, and $\dot{q}^{\mathrm{sim}}_{\mathrm{comp}}(t-1)$ the value at the previous time. Equations A-3−A-5 are applied analogously for $\dot{q}^{\mathrm{sim}}_{\mathrm{cool}}$ as a function of T_{j}. The dynamic parameters were characterised by performing experimental temperature steps on T_{r} and multiobjective optimisation. More details on experimental conditions and optimisation procedures are given elsewhere.[26]

(32) Bugnon, P.; Chottard, J.; Jestin, J.; Jung, B.; Laurenczy, G.; Maeder, M.; Merbach, A.; Zuberbühler, A. *Anal. Chim. Acta* **1994**, *298*, 193–201.
(33) Perry, R., Green, D. W., Maloney, J. O. *Perry's Chemical Engineers' Handbook*, 7th ed.; McGraw-Hill: New York, 1997.

Received for review November 12, 2009.

OP900298X